iScience

CellPress

Article

Genetically Encoded Fluorescent Indicator GRAPHIC Delineates Intercellular Connections

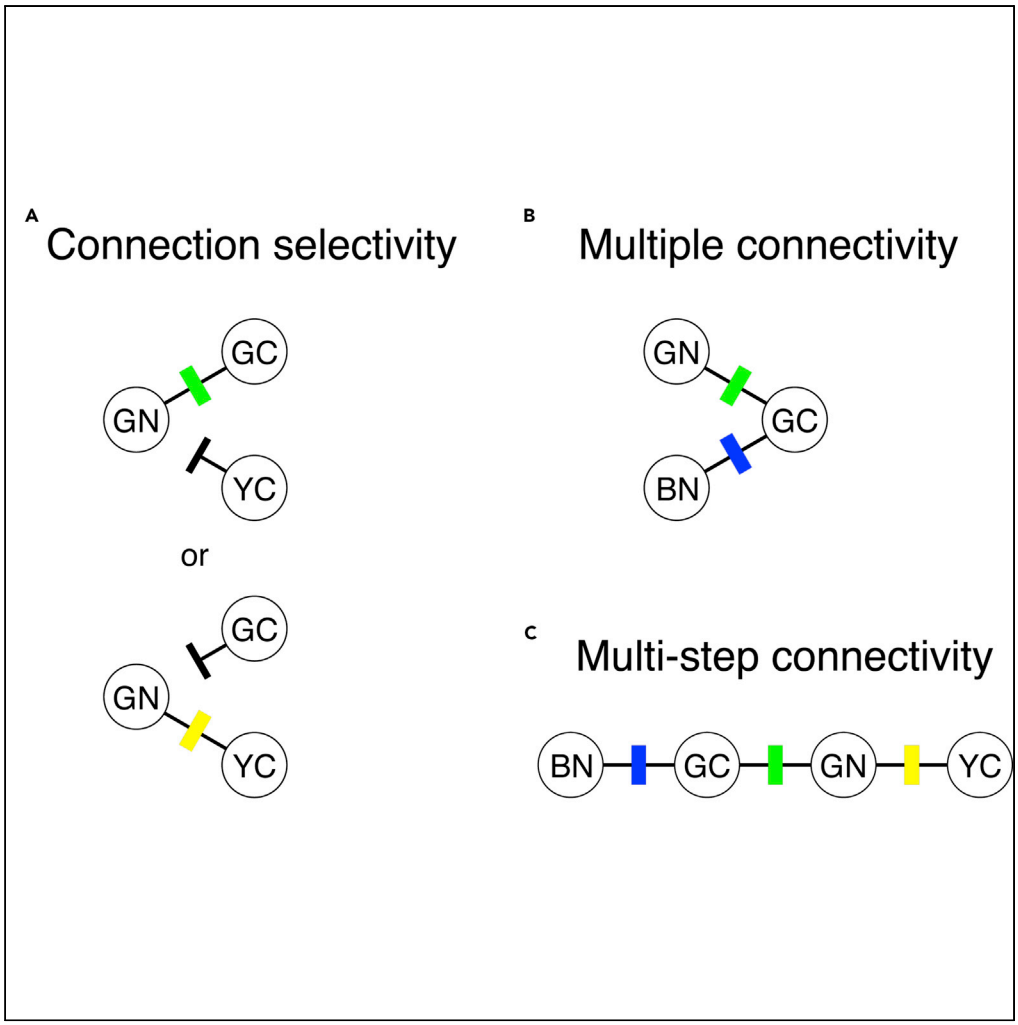

Nagatoki Kinoshita, Arthur J.Y. Huang, Thomas J. McHugh, ..., Scott H. Soderling, Atsushi Miyawaki, Tomomi Shimogori

tomomi.shimogori@riken.jp

HIGHLIGHTS

Development of GRAPHIC to visualize intercellular contact site

GPI anchor and different split site provides stronger fluorescent signal

GRAPHIC can be used to delineate synaptic site in mouse CNS and zebrafish retina

GRAPHIC color variants for multi–contact site visualization

Kinoshita et al., iScience *15*, 28–38
May 31, 2019
https://doi.org/10.1016/j.isci.2019.04.013

iScience

CellPress

Article

Genetically Encoded Fluorescent Indicator GRAPHIC Delineates Intercellular Connections

Nagatoki Kinoshita,[1,2] Arthur J.Y. Huang,[3] Thomas J. McHugh,[3] Sachihiro C. Suzuki,[4] Ichiro Masai,[4] Il Hwan Kim,[5] Scott H. Soderling,[5] Atsushi Miyawaki,[2,6] and Tomomi Shimogori[1,7,*]

SUMMARY

Intercellular contacts are essential for precise organ morphogenesis, function, and maintenance; however, spatiotemporal information of cell-cell contacts or adhesions remains elusive in many systems. We developed a genetically encoded fluorescent indicator for intercellular contacts with optimized intercellular GFP reconstitution using glycosylphosphatidylinositol (GPI) anchor, GRAPHIC (GPI anchored reconstitution-activated proteins highlight intercellular connections), which can be used for an expanded number of cell types. We observed a robust GFP signal specifically at the interface between cultured cells, without disrupting natural cell contact. Application of GRAPHIC to the fish retina specifically delineated cone-bipolar connection sites. Moreover, we showed that GRAPHIC can be used in the mouse central nervous system to delineate synaptic sites in the thalamocortical circuit. Finally, we generated GRAPHIC color variants, enabling detection of multiple convergent contacts simultaneously in cell culture system. We demonstrated that GRAPHIC has high sensitivity and versatility, which will facilitate the analysis of the complex multicellular connections without previous limitations.

INTRODUCTION

In multicellular organisms, intercellular communication controls orchestrated morphogenesis during development and functional cooperation of multiple cells. Long-range intercellular communication via secreted ligands organizes cellular functions extending over multiple tissues and organs (Baes and Denef, 1987; Pires-daSilva and Sommer, 2003), whereas direct cell-cell contact plays a crucial role in tuning more local and specific events, including polarized cell migration (Carmona-Fontaine et al., 2008; Mayor and Carmona-Fontaine, 2010), control of organ mass (McClatchey and Yap, 2012), immune system maturation (Miller and Basten, 1996; van Panhuys, 2016), and formation and plasticity of functional neural circuits (Craig and Kang, 2007; Holland et al., 1998; Varoqueaux et al., 2006). Therefore identification of specific cell-cell contacts and analysis of its physiological significances are important to investigate how each organ acquires and maintains its proper function. However, detection of transient intercellular contacts and isolation of specific interactions within intermingled multicellular networks are difficult to perform.

To address this issue, systems that visualize intercellular contacts via *trans*-cellular molecular interactions between pairs of receptor-ligand membrane proteins have been reported. The GRASP (green fluorescence protein [GFP] reconstitution across synaptic partners) system developed by the Bargmann lab employed the human T cell protein CD4 (Feinberg et al., 2008). To minimize intracellular interactions, the cytosolic domains of CD4 that interact with signaling molecules were deleted, leaving a seven-amino acid cytosolic tail; the extracellular domain was also truncated to include only one or two of its four immunoglobulin domains. This CD4::split GFP system (i.e., CD4::GFP1-10 + CD4::GFP11) has been extensively used to label many cellular contacts in *Drosophila* (Gordon and Scott, 2009; Makhijani et al., 2017; Roy et al., 2014) and transient immune synaptic contacts between T cells and antigen-presenting cells (Pasqual et al., 2018). Most of the other probe systems to identify intercellular contacts have been designed to label synaptic connections in neural circuits, based on interactions between synaptogenesis molecules, neurexin-neuroligin. ID-PRIM (interaction-dependent probe incorporation mediated by enzymes) (Liu et al., 2013) and the horseradish peroxidase reconstitution system (Liu et al., 2013; Martell et al., 2016) employ an enzyme-substrate reaction, and in GRASP (Feinberg et al., 2008) and SynView (Tsetsenis et al., 2014) systems, split GFP fragments tethered to pre- and postsynaptic membrane proteins reconstitute a GFP

[1]Molecular Mechanisms of Brain Development, Center for Brain Science (CBS), RIKEN, Saitama, Japan

[2]Exploratory Research for Advanced Technology (ERATO), Japan Science and Technology Agency (JST), Tokyo, Japan

[3]Circuit and Behavioral Physiology, CBS, RIKEN, Saitama, Japan

[4]Developmental Neurobiology Unit, Okinawa Institute of Science and Technology Graduate University (OIST), Okinawa, Japan

[5]Department of Cell Biology, Duke University Medical School, Durham, NC, USA

[6]Cell Function Dynamics, CBS, RIKEN, Saitama, Japan

[7]Lead Contact

*Correspondence: tomomi.shimogori@riken.jp

https://doi.org/10.1016/j.isci.2019.04.013

molecule in the synaptic cleft after synapse formation (Scheiffele et al., 2000). These systems are successful in isolating specific neuronal connectivity from highly heterogeneous connections among numerous neurons. However, to use these probes in the mammalian system, specific expression of probes is required in post- or presynaptic cells to reveal specific connections, which seems to be causing low expression level of probes and low signal intensity (Kim et al., 2012). To generate a simpler system, we utilized GPI (glycosylphosphatidylinositol)-anchored membrane-associated domains, which lack a cytoplasmic tail, to permit visualization via the reconstitution of split GFP (N-terminal fragment probe [NT-probe]: 1–7 within its 11 β-sheets, C-terminal fragment probe [CT-probe]: within its 11 β-sheets). Moreover, by utilizing a GFP split site distinct from the previous indicators we could dramatically increase the signal intensity. Additional optimizations of molecular structure achieved higher GFP reconstitution activity at intercellular contact sites.

Our next challenge is to engineer a color variant that will enable us to distinguish different connectivities at the same time. GFP has several color variants (blue fluorescent protein [BFP], cyan fluorescent protein [CFP], yellow fluorescent protein [YFP], etc.), and their fluorescent characteristics depend on specific point mutations (Pakhomov and Martynov, 2008; Shaner et al., 2007). Combination-dependent color variation of a GFP reconstitution system utilizes GFP diversity and is a useful application to obtain multiple data simultaneously (Hu and Kerppola, 2003).

As our probe molecules have no cell type specificity, no directionality, and no specific interacting domain for endogeneous molecules, the GRAPHIC system can be applied to many types of intercellular contacts in organisms. In the present study, we applied this system to visualize neuronal connectivity in mouse brain and zebrafish retina and demonstrated that it provides a strong signal that can specifically highlight synaptic sites. This GFP reconstitution probe will be a powerful tool to analyze specific intercellular contacts, even in highly complicated systems.

RESULTS

Design and Characterization of GRAPHIC Probes

We designed a set of GPI-anchored membrane proteins for effectively displaying two complementary GFP fragments on the plasma membrane (Figure 1A). With this strategy, fluorescent GFP molecules will be reconstituted specifically at the contact area between two cells expressing each fragment (Figure 1C). To identify the cells expressing the GFP N-terminal fragment probe (NT-probe), H2B (histone 2B)-mCherry was attached to the NT-probe with 2A self-cleavable peptide (Figure 1A). For GFP C-terminal fragment probe (CT-probe), H2B-Azurite was attached. To determine the most efficient split site of superfolder GFP (sfGFP) (Cabantous et al., 2005; Pedelacq et al., 2006), we tested the reconstitution activity of two probe pairs containing sfGFP fragments cut at 1-7/8-11 and 1-10/11 within its 11 β-sheets (Figure 1B). The 1-7/8-11 split site is frequently used in the BiFC (bimolecular fluorescence complementation) method (Kerppola, 2008; Shyu and Hu, 2008), whereas the 1-10/11 split site is used for all previous intercellular probes (Feinberg et al., 2008; Kim et al., 2012; Tsetsenis et al., 2014). In this system, we found that the 1-7/8-11 combination possessed higher reconstitution activity than the 1-10/11 combination (Figure S1). Moreover, because there are no endogeneous receptor-ligand molecular interactions in the system, we introduced a leucine zipper domain in both NT- and CT-probes as to facilitate GFP reconstitution (Figure 1A). We fused an acidic leucine zipper domain to the NT-probe and basic leucine zipper domain to the CT-probe, to promote *trans*-molecular (acidic-basic) over *cis*-molecular (acidic-acidic or basic-basic) interactions (O'Shea et al., 1993). This probe contains an N-terminal mouse preproacrosin signal peptide (24 amino acids [aa]: SP) followed by a split-GFP fragment, leucine zipper domain, and mouse Thy-1 GPI anchor domain (C-terminal 31 aa) (Figure 1A). Based on the design of the probe, we named it GRAPHIC (GPI anchored reconstitution-activated proteins highlight intercellular connections), with the notation of NT- and CT-probes as n- and c-GRAPHIC, respectively.

To test the sensitivity of GRAPHIC and to compare with other indicators for mammalian intercellular contacts, we first assessed the GRAPHIC and mGRASP systems (the mammalian variant of the GRASP system) in epithelial cells (LLCPK1) (Figure 2A). All GRAPHIC and mGRASP probes were co-expressed with nucleic fluorescent labels for normalization of probe expression level. GRAPHIC showed a strong signal at the cell-cell contact sites, whereas there was no significant signal observed in mGRASP under identical imaging conditions. To test whether change of GFP split site also affects mGRASP signal intensity, we generated modified mGRASP with 1-7/8-11 sfGFP fragments instead of the original 1-10/11 fragments. Although the modified mGRASP significantly increased signal intensity, it was still much weaker than GRAPHIC

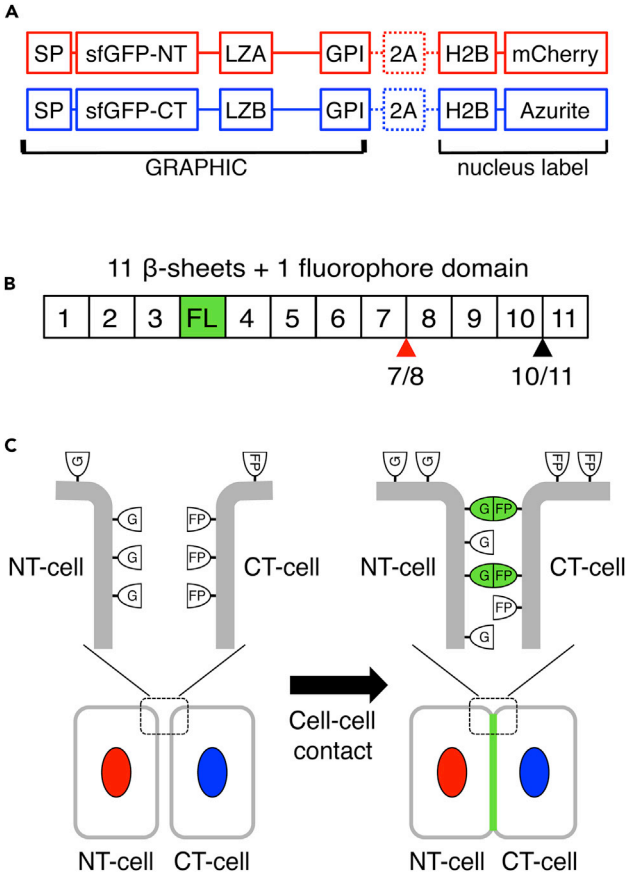

Figure 1. Design of GRAPHIC and Its Signal Pattern

(A) Diagram of GRAPHIC molecular structures. GRAPHIC molecules consist of signal peptide (SP), split sfGFP fragment, leucine zipper domains (LZA or LZB), and GPI anchor domain. To identify and estimate probe expression, H2B-mCherry and H2B-Azurite were co-expressed with NT-probe and CT-probe, respectively.

(B) GFP molecule consists of 11 β-sheets and fluorophore domain (FL). sfGFP split site for GRAPHIC is between seventh and eighth β-sheet (7/8). Other intercellular probe systems utilize 10/11 split site.

(C) Diagram of GRAPHIC labeling intercellular contact. GFP molecules are reconstituted by intercellular interaction of a set of probe molecules at cell-cell contact site.

(Figure 2). As mGRASP is designed to express most efficiently in neurons, it is possible that the improved GRAPHIC signal is specific to LLCPK1 cells. To test this, we used a mouse neuroblastoma cells line, N2A cells, to express both probes and observed similar results (data not shown). These results demonstrate that the 1-7/8-11 GFP split site, the unique leucine zipper interaction, and GPI anchor tethering of GRAPHIC provides higher signal intensity than the GRASP system, suggesting that GRAPHIC may be a more sensitive indicator for intercellular interactions to visualize cell-cell contact domain.

Spatiotemporal Dynamics of GRAPHIC Signal

To quantify the speed of GFP reconstitution by GRAPHIC, we performed time-lapse imaging using the LLCPK1 cell line. An initial GRAPHIC signal was detected 1 h after cell-cell contact, and its intensity gradually increased at cell-cell contact sites over 12 h (Figure 3A and Video S1). To determine the GRAPHIC signal stability, we next observed GRAPHIC signal dynamics when intercellular contacts were disrupted by ion chelation (Figure 3B, Video S2, Figure S2). Time-lapse imaging revealed that the GRAPHIC signal was not abolished, but still remained on retracted plasma membrane of n- and c-GRAPHIC-expressing cells for at least 1 h after ion chelation. Although GRAPHIC signal complexes are formed at cell-cell contact sites, its robustness may artificially strengthen cell adhesion. To address this issue, we estimated cell detachment rates of LLCPK1 cells with and without expression of GRAPHIC molecules and could not observe significant effect of GRAPHIC on cell adhesion (Figure 3C). Considering that formation of

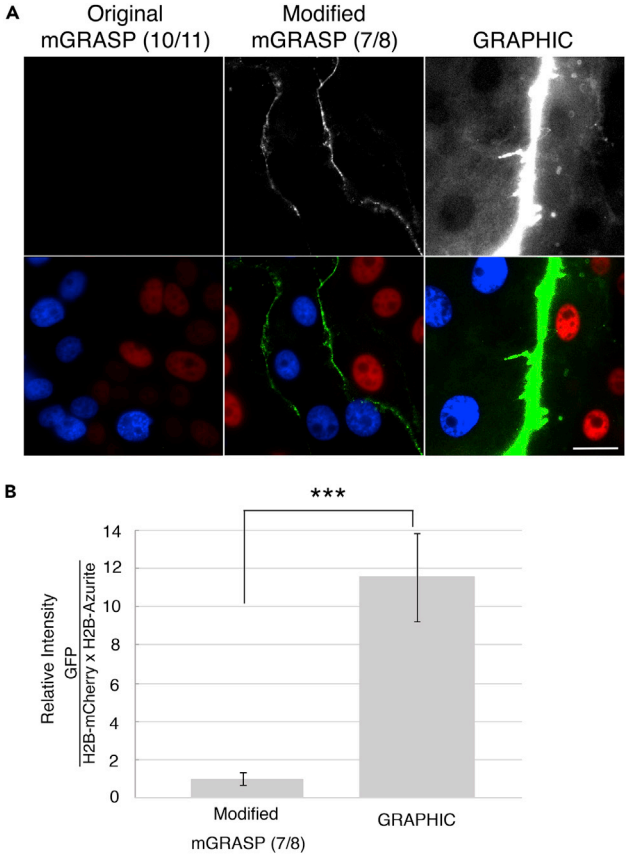

Figure 2. Comparison of GRAPHIC with Other Probes

(A) GRAPHIC showed higher signal intensity in LLCPK1 epithelial cell culture. Modification of GFP split site (10/11 to 7/8) in mGRASP system increased its signal intensity. All three culture and image acquisition conditions are same.

(B) Quantification and comparison of GRAPHIC (n = 57) and modified mGRASP (7/8) (n = 66) signal intensity. GFP signals were normalized with co-expressed nuclei label intensities of contacted cells. GFP-NT fragment (post-mGRASP and n-GRAPHIC)-expressing cells are red nuclei (H2B-mCherry, attached with 2A peptide) and GFP-CT fragment (pre-mGRASP and c-GRAPHIC)-expressing cells are blue nuclei (H2B-Azurite, attached with 2A peptide). ***$p = 1.09 \times 10^{-24}$; Student's unpaired t test. Scale bars, 20 μm.

juxtamembrane complexes and anchoring to the cytoskeleton are necessary for adhesion molecules, such as cadherins, to function effectively (Leshchyns'ka and Sytnyk, 2016; Yonemura, 2017), GRAPHIC is unlikely to generate significant force at cell-cell contact sites due to its lack of intracellular domain. Moreover, fluorescence-activated cell sorting analysis showed that the GRAPHIC signals induced by co-culturing the two cell populations were detectable after complete cell dissociation (Figures 3D–3F). These results indicate that GRAPHIC has specific GFP reconstitution activity at cell-cell contact sites, and its signal complex is stable and can remain on either cell until it is degraded even after dissolution of the intercellular contacts.

Color Multiplexing of GRAPHIC

Tissues and organs consist of heterogeneous cell types, therefore, to clarify their developmental and functional mechanisms, identification of contact specificity and selectivity among multiple cells is important. Multicolored labeling is an advantageous strategy to detect multiple contacts simultaneously, and combination dependency of multicolored BiFC method (Hu and Kerppola, 2003) is suitable for identification of contact selectivity, therefore we developed GRAPHIC color variants.

GFP has several color variants (BFP, CFP, YFP, etc.), and their fluorescent characteristics depend on specific point mutations (Pakhomov and Martynov, 2008; Shaner et al., 2007). Combination-dependent color

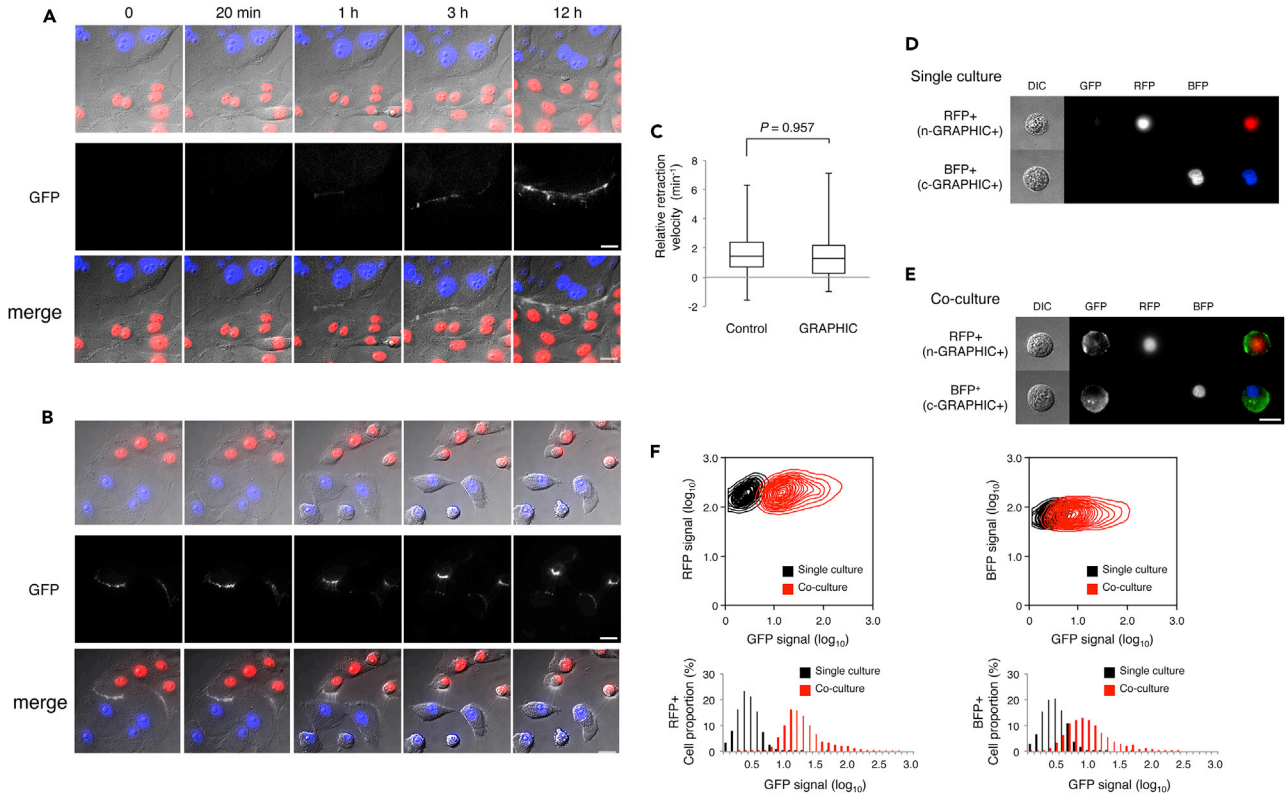

Figure 3. Characteristics of GRAPHIC Signal

(A and B) Time-lapse images of GRAPHIC signal in constructing (A) or disrupting (B) intercellular contact between n-GRAPHIC-expressing LLCPK1 cells (red nuclei) and c-GRAPHIC-expressing LLCPK1 cells (blue nuclei). Upper panels are merged images of bright-field (differential interference contrast), RFP and BFP fluorescence. Bottom panels are GFP fluorescent images. In (A), two cell lines first contacted at time 0. In (B), EDTA was administrated at time 0 (final concentration; 5mM).

(C) Quantification of relative membrane retraction velocity during 10–12 min after EDTA ion chelation. H2B-mCherry-expressing (without GRAPHIC) LLCKP1 cells ($n = 51$) were used as control. Membrane retraction velocity of GRAPHIC was calculated between n- and c-GRAPHIC-expressing cells ($n = 33$). Student's unpaired t test.

(D-F) GRAPHIC signal still remains in completely dissociated cells. Dissociated (with 5 mM EDTA, without trypsin) LLCPK1 cells from single culture of RFP+ (n-GRAPHIC expressing) or BFP+ (c-GRAPHIC expressing) cell line and co-culture of both cell lines were subjected to flow cytometry (single cultured RFP+; $n = 4751$, single cultured BFP+; $n = 4851$, co-cultured RFP+; $n = 6062$, co-cultured BFP+; $n = 5131$). Both microscope observation (D and E) and histogram of GFP intensity (F) of sorted cells showed co-culture dependent GRAPHIC signal in dissociated single cell. Scale bars, 20 μm.

variation of a GFP reconstitution system utilizes GFP diversity and is a useful application to obtain multiple data simultaneously (Hu and Kerppola, 2003). Considering that the critical mutation for BFP is within the GFP 1-7 fragment, and for YFP, within the GFP 8-11 fragment, we designed these color probe molecules (XFP-NT (XN), XFP-CT (XC)) and tested them in LLCPK1 cells. As expected, reconstituted signal between BN-probe-expressing cells and GC-probe-expressing cells showed blue fluorescence, which is distinguishable from GFP reconstitution (Figures 4A–4C). Next, we tested CT-probe-dependent color variant, and the reconstitution signal of GN- and YC-probe clearly showed a fluorescent spectrum shift from GFP to YFP (Figures 4D–4H). Thus, we generated distinguishable GRAPHIC color variants, which can visualize combinations of connected cell types. Also, distinct from previous indicators, GRAPHIC provides NT-probe- or CT-probe-dependent color variant. This enables us to identify which connections have been selected among many prospective candidates by observation of the color of contacted sites.

To clarify the patterns of highly heterogeneous connections, the simultaneous detection of multiple convergent connections upon single cells is crucial. For multicolored display of multiple intercellular connections in one cell, we co-cultured cells transfected with GN-, GC-, and YC-probe into red (H2B-mCherry), colorless, and blue (H2B-Azurite) nuclei LLCPK1 cells, respectively. At the junctions of these three cell types, reconstituted signals showed GFP fluorescent characteristics at GN-GC contact site and YFP

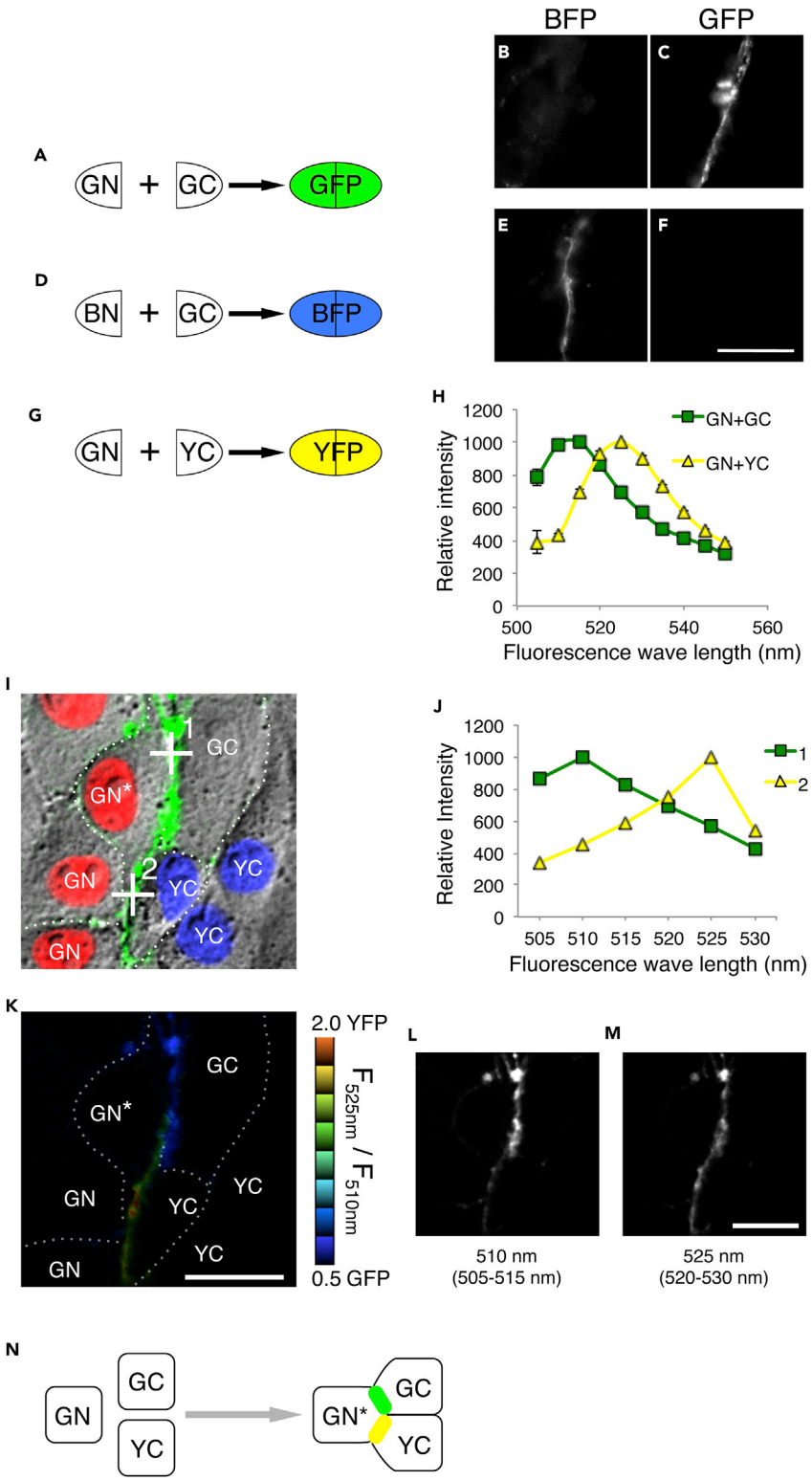

Figure 4. Development of Color Variants of GRAPHIC

(A–F) Fluorescent character of BFP is mainly dependent on GFP-NT fragment region (GFP 1-7). Substitution of eight amino acid residues in GFP 1-7, I39N, T65S, Y66H, S72A, K105T, T128V, V150I, D155V altered the fluorescent character of reconstituted signal, GFP to BFP. GFP-type combination (GN + GC) signal at cell-cell contact sites of LLCPK1 could be

Figure 4. *Continued*

detected with microscope filter set for GFP detection (excitation 465-485 nm, emission 502-534 nm) (C), but not for BFP (excitation 355-405 nm, emission 420-480 nm) (B), whereas BFP-type combination (BN + GC) signal could be detected with microscope filter set for BFP (E), but not for GFP (F).

(G and H) Fluorescent character of YFP is mainly dependent on T203I amino acid substitution of GFP, which is within GFP-CT fragment region (GFP 8-11). (H) Comparing fluorescent spectrums at cell-cell contact sites of GFP- (GN + GC) and YFP-type combination (GN + YC), T203I substitution in GFP 8-11 domain of c-GRAPHIC shifted reconstituted signal character to YFP-like longer wavelength. Error bars, ± SD.

(I–N) Co-culture of three LLCPK1 cell lines (GN cells express n-GRAPHIC and H2B-mCherry, GC cells express only c-GRAPHIC, and YC cells express YFP type c-GRAPHIC and H2B-Azurite) showed that the GRAPHIC system simultaneously detected multiple connectivity in one cell. (I) GN* cell contacts with both GC cell and YC cell. (J) Fluorescent spectra at points 1 and 2 showed GFP-like and YFP-like characters, respectively. (K) Ratiometric image of reconstituted signal intensities at 510 nm (gated 505–515 nm) (L) and 525 nm (gated 520–530 nm) (M). GN* cell contacts with both GC cell and YC cell, and each contact region can be separated by its fluorescent character (K and N). Scale bars, 20 μm.

characteristics at GN-YC contact site (Figures 4I–4M). Even in one cell, GRAPHIC color variants clearly showed individual contact sites with different colors suggesting that multiple types of intercellular connections, such as multistep connections and multiple convergent connections, may be separated and identified simultaneously (Figure 4N).

Taken together, further development of color variant GRAPHIC has the possibility of being a powerful tool to investigate multiple heterogeneous connections in multicellular organisms.

GRAPHIC Enables the Visualization of Neuronal Connectivity

We have shown that GRAPHIC delineates cell-cell contact site efficiently and precisely *in vitro*. To further investigate whether GRAPHIC can be used in specific intercellular contacts *in vivo*, we first tested GRAPHIC in cone-bipolar cell connections in the zebrafish retina, whose connectivity is well known (Figure 5A). n-GRAPHIC and membrane-targeted tdTomato were co-expressed in bipolar cells (vsx1 promoter, Randlett et al., 2013), whereas c-GRAPHIC and mTagBFP2 were co-expressed in cone cells (gnat2 gene promoter, Kennedy et al., 2007) (Figure 5A). In 5 days postfertilization retina, GRAPHIC fluorescence was only observed within the synaptic region where the dendritic tips of tdTomato-positive bipolar cells associated with mTagBFP-positive cone pedicles (Figure 5B). Next, we applied GRAPHIC to mouse central nervous system (CNS) to test if GRAPHIC can detect specific synaptic site in more complicated neuronal circuit. Considering in highly myelinated neural circuits, neuron-neuron contact areas are known to be mostly limited to synapses. Therefore it will be a good system to test the specificity of GRAPHIC in CNS to detect synapses without carrying synaptic localization signal. First, we tested localization of GRAPHIC signal in the synapses of the mouse thalamocortical circuit. The primary somatosensory cortex (S1) layer IV neurons receive dense innervation of thalamocortical axons (TCAs) from the ventrobasal (VB) thalamus and form synaptic connections (Lopez-Bendito and Molnar, 2003; Wu et al., 2011), making this an ideal circuit to assess the ability of GRAPHIC to delineate synaptic connections. To label cortical and thalamocortical neurons, *in utero* electroporation (IUE) and Adeno-associated Virus (AAV) injection were performed, respectively (Figure 5C). Cortical layer neurons are transfected n-GRAPHIC-2A-H2B-mCherry by IUE at embryonic day (E) 13.5. At 2–3 weeks after birth electroporated mice were stereotaxically injected with c-GRAPHIC-2A-mCherry encoding AAV into the VB thalamus. Transfected neurons, visualized by nuclear-localized mCherry, were distributed in cortex, mostly in layer IV (Figure 5D left). Transfected neurons are seen in the VB thalamus by mCherry signal, and TCAs were detected by a diffuse mCherry signal in the thalamus (Figure 5D right, arrows) and cortical layer IV (Figure 5D left, bracket). Confocal images of cortical layer IV showed scattered GFP signal along mCherry-positive TCAs surrounding mCherry-positive bouton-like structures (Figure 5E, arrowheads). Interestingly there are no synaptic boutons in layer V and no GRAPHIC signal on mCherry-positive TCA in layerV, which suggest synapse specific GFP reconstitution by GRAPHIC. These results suggest that GFP reconstitution only occurs in specific regions, most likely postsynaptic sites. To test this more directly we replaced H2B-mCherry with PSD95-mCherry in n-GRAPHIC to label the postsynaptic density. Cortical neurons were transfected n-GRAPHIC-2A-PSD95-mCherry by IUE at E13.5. To distinguish mCherry-labeled TCA terminals and PSD95-mCherry signal in cortex, VB neurons were labeled by c-GRAPHIC-2A-H2B-mCherry encoding AAV for this experiment (Figure 5F). In confocal images of cortical layer IV we observed a punctate GRAPHIC GFP signal, which largely overlapped with the PSD95-mCherry labeled postsynaptic sites (83.1% ± SD 4.5%, 12 regions of 2 animals) (Figure 5G). The GFP puncta, which did not co-localize

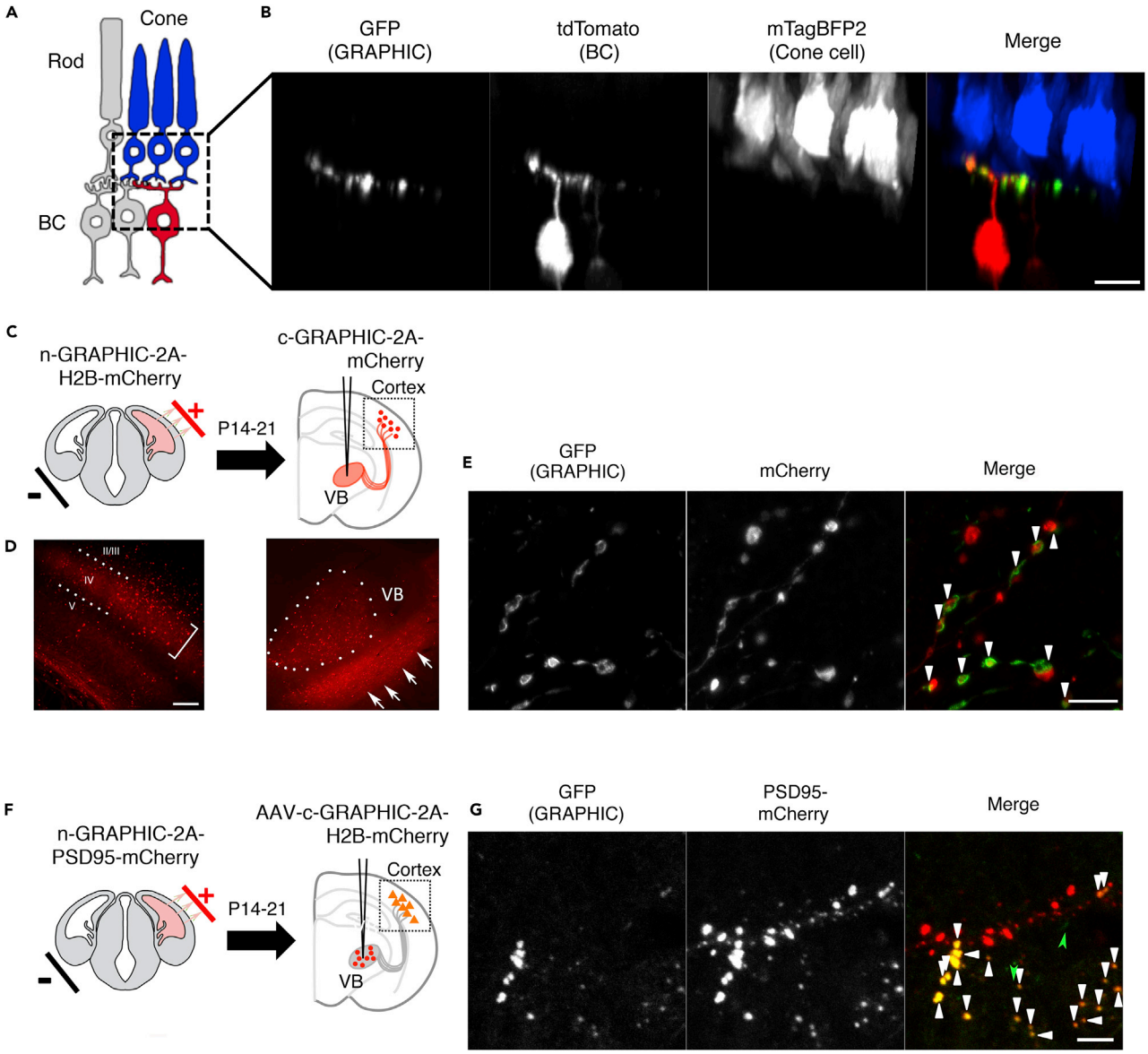

Figure 5. GRAPHIC Visualizes Synaptic Connection in Neuronal Networks

(A and B) GRAPHIC labels synaptic sites in zebrafish retina. (A) In the zebrafish retina, typical structures, ribbon synapses, are formed between cone photoreceptor axon terminals, namely, pedicles and dendrites of bipolar cells. n-GRAPHIC and membrane-targeted tdTomato were co-expressed in a subpopulation of bipolar cells using the vsx1 promoter (*vsx1*: *memtdTomato-2A-n-GRAPHIC*), and c-GRAPHIC and TagBFP2 were co-expressed in cone cells using the *guanine nucleotide-binding protein G(t) subunit alpha-2* (*gnat2*) gene promoter (*gnat2*: *TagBFP2-2A-c-GRAPHIC*). Both expression vectors were co-injected into one-cell-stage zebrafish embryos and then fixed at 5 days postfertilization. (B) Reconstituted GFP signals were only detected at the dendritic tips of tdTomato-positive bipolar cell closely associated with TagBFP2-expressing cone pedicle. Scale bar, 5 μm.

(C–E) GRAPHIC signals in S1 layer IV neurons are merged with thalamocortical axons of VB neurons in mouse brain. (C) *In utero* electroporation (IUE) was performed at E13.5–14.5 to express n-GRAPHIC-2A-H2B-mCherry in cortical layer IV. After the electroporated mice had grown up to P14-21, c-GRAPHIC-2A-mCherry encoding AAV was stereotaxically injected into VB. After 30–40 days, the injected brains were sectioned and observed. (D) Certain number of cortical layer IV neurons (bracket) expressed n-GRAPHIC (indicated by co-expressed red nuclei label, dot line) and many mCherry labeled fibers of c-GRAPHIC expressing VB neurons reached to cortical layer IV (white arrows). (E) Higher magnification of confocal images of layer IV showed many GFP puncta largely overlapped with mCherry-positive bouton-like structures. GFP puncta that co-localize with mCherry-positive axons are indicated by arrowheads. Scale bars, 200 μm in (D) and 5 μm in (E).

(F) IUE was performed at E13.5 to express n-GRAPHIC-2A-PSD95-mCherry in cortical layer IV. After the electroporated mice had grown to adult (about 2-month-old), c-GRAPHIC-2A-H2B-mCherry encoding AAV was stereotaxically injected into thalamus VB. After about 4 weeks, the injected brains were sectioned and observed.

Figure 5. *Continued*
(G) Distribution of GRAPHIC signals in cortical layer IV neurons. GFP (GRAPHIC) signals indicate contacted sites between n-GRAPHIC-expressing layer IV neurons and c-GRAPHIC-expressing VB neurons. PSD95-mCherry signals indicate postsynaptic sites of electroporated layer IV neurons. GFP puncta that co-localize with PSD95-mCherry puncta are indicated by arrowheads. Scale bar, 5 μm.

with PSD-95, were smaller in size than those that overlapped (Figure 5G, green arrow heads), suggesting these are possibly immature synapses or residual GRAPHIC signal of disrupted synapses. Finally, to test whether GRAPHIC has preference for pre- or postsynaptic neurons, we swapped the position of n-GRAPHIC (VB: presynaptic) and c-GRAPHIC (cortical neurons: postsynaptic) (Figure 5C) and observed staining patterns identical to those seen in Figure 5E (data not shown). These experiments demonstrate that GRAPHIC shows strong GFP reconstitution activity without any orientation preference for pre- or postsynaptic neurons.

Taken together, GRAPHIC is a robust approach to delineate the synaptic connections in various neural circuits of various vertebrates, and thus GRAPHIC will be a useful tool to analyze the complex connectivity *in vivo*.

DISCUSSION

Here we have generated a fluorescent probe system, GRAPHIC, which highlights specific intercellular interactions based on contact-dependent GFP reconstitution. The GRAPHIC system does not utilize cell-type-specific molecular interactions, and its unique and optimized molecular structure showed high GFP reconstitution activity. Moreover, color variant GRAPHICs revealed specific junctions between different pairs of cells depending on probe combinations. In this study, we demonstrated that GRAPHIC could be applied to the visualization of synaptic connectivity in neural circuits of different vertebrates. We anticipate that this will enable the identification of specific intercellular contacts in highly heterogeneous multicellular interactions of various tissues and animals.

The molecular structure of GRAPHIC is distinct from previous probes designed for detecting vertebrate intercellular contact with GFP reconstitution. GRAPHIC utilized 1-7/8-11 split sfGFP, whereas all other *trans*-synaptic GFP reconstitution probes utilize 1-10/11 split site (Feinberg et al., 2008; Kim et al., 2012; Tsetsenis et al., 2014). Our present study revealed that the 1-7/8-11 split pair in the mGRASP system (mGRASP(7/8)) showed higher reconstitution activity than 1-10/11 split pair. In the detection of intracellular molecular interactions, 1-7/8-11 is the most popular split site owing to its higher reconstitution activity, although it may increase non-specific molecular interactions (Kerppola, 2008; Shyu and Hu, 2008). To detect intercellular contacts, however, GFP is theoretically not reconstituted unless the cell-cell distance becomes close enough for intercellular molecular interaction. Therefore higher reconstitution activity is desirable for the visualization of intercellular connectivity, especially when its contact area is small or its contact duration is short.

While the selection of the GFP split site is a major factor for the improved signal intensity in GRAPHIC, other optimizations contribute to its increased sensitivity. The GPI anchor domain promotes effective membrane display of GRAPHIC molecules, and the leucine zipper domain facilitates GFP reconstitution from split fragments. In the comparison of reconstitution activity with modified mGRASP (7/8), these unique molecular structures showed their superiority for intercellular GFP reconstitution.

For labeling synaptic connections, all other probes utilize a pair of pre- and postsynaptic membrane proteins, neurexin and neuroligin (Feinberg et al., 2008; Kim et al., 2012; Liu et al., 2013; Martell et al., 2016; Tsetsenis et al., 2014), which clearly label precise synaptic sites (Choi et al., 2018). However, utilization of intact cytoplasmic domains of neurexin and neuroligin may generate artificial pre- and postsynaptic complexes and affect synaptic morphogenesis (Biederer and Sudhof, 2001; Craig and Kang, 2007; Irie et al., 1997). In the GRAPHIC system, the lack of a cytoplasmic domain prevents such complex formation, whereas its extracellular region is designed specifically for interactions between GRAPHIC molecules, minimizing disruption of intercellular signaling. Furthermore, GRAPHIC has no preferential cell types, allowing us to label not only neuron-neuron interactions but also potentially neuron-glia or glia-glia interactions. Furthermore, GRAPHIC could be applied to the detection of intercellular contacts in other systems, such as thymic education of T cells or cell adhesion changes in carcinogenesis. In addition, the remaining GRAPHIC signal after cell dissociation (Figures 3B and 5F) may be utilized to record past transient intercellular interactions.

Thus the unique molecular structure of GRAPHIC enables its broad versatility in the investigation of diverse intercellular contacts.

In this study, we showed that the GRAPHIC system visualized synaptic connections in different species and organs with various gene expression systems. Although this system has no synaptic localization signal, in myelinated neural circuits, GRAPHIC delineated intercellular connections between neurons. In the zebrafish retina, GRAPHIC signal specifically accumulated within the synaptic region between cone and bipolar cells. Furthermore, in mouse brain, a large population of GRAPHIC signal co-localized with synaptic sites in S1 layer IV (Figures 5C–5G). These results indicate that GRAPHIC can be a widely effective method to investigate *in vivo* connectivity of vertebrate nervous systems.

GRAPHIC is also capable of analyzing higher-order connectivity consisting of more than three cell types with its combination-dependent color variation. We generated both NT-probe-dependent variant (BFP) and CT-probe-dependent variant (YFP). Considering that the essential amino acid substitutions for some GFP variants (e.g., YFP, Sapphire, Ehrig et al., 1995) are in 10th β-sheet, the 1-7/8-11 split site allows us to generate CT-probe-dependent color variants. This multicolor combinatorial variety makes it possible to identify contact selectivity and detect multiple convergent connections and multistep connectivity. These GRAPHIC technical features will be important to clarify the heterogeneous complex cell-cell connections. Together with higher sensitivity and successful visualization of *in vivo* neural circuit connectivity, GRAPHIC will be a useful tool to analyze various intercellular contacts, especially within highly complicated systems, such as the nervous system.

Limitations of Study

As GRAPHIC does not have synapse localization signal, we do not know if it can be used in developing brains to visualize newly formed synapses.

METHODS

All methods can be found in the accompanying Transparent Methods supplemental file.

SUPPLEMENTAL INFORMATION

Supplemental Information can be found online at https://doi.org/10.1016/j.isci.2019.04.013.

ACKNOWLEDGMENTS

We thank G. Kondoh (Kyoto University) for cDNAs of mouse preproacrosin signal peptide and mouse Thy-1 GPI-anchored domain, T. Kanda (Aichi Cancer Center Research Institute) for cDNA of human histone H2B, R. Tsien (UC San Diego) for cDNA of mCherry, S. Yonemura (RIKEN CDB) for LLCPK1 cell, and H. Miyoshi (RIKEN BRC) for lentiviral vectors. We thank T.R. Young for comments on this paper, S.S. Kikuchi for animal care, and A.C. Yoshida for technical assistance. This work was supported by the RIKEN CBS (to T.J.M., A.M., and T.S.) and OIST (to I.M.). This work was supported by ERATO-JST (to A.M.), Grant-in-Aid for Scientific Research on Innovative Areas "Dynamic regulation of brain function by Scrap &Build system," 16H06459 (T.S.), and Japan Society for the Promotion of Science (JSPS) KAKENHI Grant Number 15K14329 (to N.K.).

AUTHOR CONTRIBUTIONS

N.K. designed GRAPHIC components and performed cell biological assays, animal surgery, imaging, and data analysis. A.J.Y.H. and T.J.M. developed AAV and performed stereotaxic injections. I.H.K. and S.H.S. performed contralateral S1 connection experiment. S.C.S. and I.M. performed zebrafish retina experiment. N.K., A.M., and T.S. wrote the paper. All authors discussed and commented on the manuscript.

DECLARATION OF INTERESTS

The authors declare no competing financial interest.

Received: January 21, 2019
Revised: February 5, 2019
Accepted: April 6, 2019
Published: May 31, 2019

REFERENCES

Baes, M., and Denef, C. (1987). Evidence that stimulation of growth hormone release by epinephrine and vasoactive intestinal peptide is based on cell-to-cell communication in the pituitary. Endocrinology *120*, 280–290.

Biederer, T., and Sudhof, T.C. (2001). CASK and protein 4.1 support F-actin nucleation on neurexins. J. Biol. Chem. *276*, 47869–47876.

Cabantous, S., Terwilliger, T.C., and Waldo, G.S. (2005). Protein tagging and detection with engineered self-assembling fragments of green fluorescent protein. Nat. Biotechnol. *23*, 102–107.

Carmona-Fontaine, C., Matthews, H.K., Kuriyama, S., Moreno, M., Dunn, G.A., Parsons, M., Stern, C.D., and Mayor, R. (2008). Contact inhibition of locomotion in vivo controls neural crest directional migration. Nature *456*, 957–961.

Choi, J.H., Sim, S.E., Kim, J.I., Choi, D.I., Oh, J., Ye, S., Lee, J., Kim, T., Ko, H.G., Lim, C.S., et al. (2018). Interregional synaptic maps among engram cells underlie memory formation. Science *360*, 430–435.

Craig, A.M., and Kang, Y. (2007). Neurexin-neuroligin signaling in synapse development. Curr. Opin. Neurobiol. *17*, 43–52.

Ehrig, T., O'Kane, D.J., and Prendergast, F.G. (1995). Green-fluorescent protein mutants with altered fluorescence excitation spectra. FEBS Lett. *367*, 163–166.

Feinberg, E.H., Vanhoven, M.K., Bendesky, A., Wang, G., Fetter, R.D., Shen, K., and Bargmann, C.I. (2008). GFP reconstitution across synaptic partners (GRASP) defines cell contacts and synapses in living nervous systems. Neuron *57*, 353–363.

Gordon, M.D., and Scott, K. (2009). Motor control in a Drosophila taste circuit. Neuron *61*, 373–384.

Holland, S.J., Peles, E., Pawson, T., and Schlessinger, J. (1998). Cell-contact-dependent signalling in axon growth and guidance: Eph receptor tyrosine kinases and receptor protein tyrosine phosphatase β. Curr. Opin. Neurobiol. *8*, 117–127.

Hu, C.D., and Kerppola, T.K. (2003). Simultaneous visualization of multiple protein interactions in living cells using multicolor fluorescence complementation analysis. Nat. Biotechnol. *21*, 539–545.

Irie, M., Hata, Y., Takeuchi, M., Ichtchenko, K., Toyoda, A., Hirao, K., Takai, Y., Rosahl, T.W., and Sudhof, T.C. (1997). Binding of neuroligins to PSD-95. Science *277*, 1511–1515.

Kennedy, B.N., Alvarez, Y., Brockerhoff, S.E., Stearns, G.W., Sapetto-Rebow, B., Taylor, M.R., and Hurley, J.B. (2007). Identification of a zebrafish cone photoreceptor-specific promoter and genetic rescue of achromatopsia in the nof mutant. Invest. Ophthalmol. Vis. Sci. *48*, 522–529.

Kerppola, T.K. (2008). Bimolecular fluorescence complementation: visualization of molecular interactions in living cells. Methods Cell Biol. *85*, 431–470.

Kim, J., Zhao, T., Petralia, R.S., Yu, Y., Peng, H., Myers, E., and Magee, J.C. (2012). mGRASP enables mapping mammalian synaptic connectivity with light microscopy. Nat. Methods *9*, 96–102.

Leshchyns'ka, I., and Sytnyk, V. (2016). Reciprocal interactions between cell adhesion molecules of the immunoglobulin superfamily and the cytoskeleton in neurons. Front. Cell Dev. Biol. *4*, 9.

Liu, D.S., Loh, K.H., Lam, S.S., White, K.A., and Ting, A.Y. (2013). Imaging trans-cellular neurexin-neuroligin interactions by enzymatic probe ligation. PLoS One *8*, e52823.

Lopez-Bendito, G., and Molnar, Z. (2003). Thalamocortical development: how are we going to get there? Nat. Rev. Neurosci. *4*, 276–289.

Makhijani, K., Alexander, B., Rao, D., Petraki, S., Herboso, L., Kukar, K., Batool, I., Wachner, S., Gold, K.S., Wong, C., et al. (2017). Regulation of Drosophila hematopoietic sites by Activin-beta from active sensory neurons. Nat. Commun. *8*, 15990.

Martell, J.D., Yamagata, M., Deerinck, T.J., Phan, S., Kwa, C.G., Ellisman, M.H., Sanes, J.R., and Ting, A.Y. (2016). A split horseradish peroxidase for the detection of intercellular protein-protein interactions and sensitive visualization of synapses. Nat. Biotechnol. *34*, 774–780.

Mayor, R., and Carmona-Fontaine, C. (2010). Keeping in touch with contact inhibition of locomotion. Trends Cell Biol. *20*, 319–328.

McClatchey, A.I., and Yap, A.S. (2012). Contact inhibition (of proliferation) redux. Curr. Opin. Cell Biol. *24*, 685–694.

Miller, J.F.A.P., and Basten, A. (1996). Mechanisms of tolerance to self. Curr. Opin. Immunol. *8*, 815–821.

O'Shea, E.K., Lumb, K.J., and Kim, P.S. (1993). Peptide 'Velcro': design of a heterodimeric coiled coil. Curr. Biol. *3*, 658–667.

Pakhomov, A.A., and Martynov, V.I. (2008). GFP family: structural insights into spectral tuning. Chem. Biol. *15*, 755–764.

Pasqual, G., Chudnovskiy, A., Tas, J.M.J., Agudelo, M., Schweitzer, L.D., Cui, A., Hacohen, N., and Victora, G.D. (2018). Monitoring T cell-dendritic cell interactions in vivo by intercellular enzymatic labelling. Nature *553*, 496–500.

Pedelacq, J.D., Cabantous, S., Tran, T., Terwilliger, T.C., and Waldo, G.S. (2006). Engineering and characterization of a superfolder green fluorescent protein. Nat. Biotechnol. *24*, 79–88.

Pires-daSilva, A., and Sommer, R.J. (2003). The evolution of signalling pathways in animal development. Nat. Rev. Genet. *4*, 39.

Randlett, O., MacDonald, R.B., Yoshimatsu, T., Almeida, A.D., Suzuki, S.C., Wong, R.O., and Harris, W.A. (2013). Cellular requirements for building a retinal neuropil. Cell Rep. *3*, 282–290.

Roy, S., Huang, H., Liu, S.M., and Kornberg, T.B. (2014). Cytoneme-mediated contact-dependent transport of the drosophila decapentaplegic signaling protein. Science *343*, 1244624.

Scheiffele, P., Fan, J.H., Choih, J., Fetter, R., and Serafini, T. (2000). Neuroligin expressed in nonneuronal cells triggers presynaptic development in contacting axons. Cell *101*, 657–669.

Shaner, N.C., Patterson, G.H., and Davidson, M.W. (2007). Advances in fluorescent protein technology. J. Cell Sci. *120*, 4247–4260.

Shyu, Y.J., and Hu, C.D. (2008). Fluorescence complementation: an emerging tool for biological research. Trends Biotechnol. *26*, 622–630.

Tsetsenis, T., Boucard, A.A., Arac, D., Brunger, A.T., and Sudhof, T.C. (2014). Direct visualization of trans-synaptic neurexin-neuroligin interactions during synapse formation. J. Neurosci. *34*, 15083–15096.

van Panhuys, N. (2016). TCR signal strength alters T-DC activation and interaction times and directs the outcome of differentiation. Front. Immunol. *7*, 6.

Varoqueaux, F., Aramuni, G., Rawson, R.L., Mohrmann, R., Missler, M., Gottmann, K., Zhang, W., Südhof, T.C., and Brose, N. (2006). Neuroligins determine synapse maturation and function. Neuron *51*, 741–754.

Wu, C.S., Ballester Rosado, C.J., and Lu, H.C. (2011). What can we get from 'barrels': the rodent barrel cortex as a model for studying the establishment of neural circuits. Eur. J. Neurosci. *34*, 1663–1676.

Yonemura, S. (2017). Actin filament association at adherens junctions. J. Med. Invest. *64*, 14–19.

ISCI, Volume *15*

Supplemental Information

Genetically Encoded Fluorescent Indicator GRAPHIC Delineates Intercellular Connections

Nagatoki Kinoshita, Arthur J.Y. Huang, Thomas J. McHugh, Sachihiro C. Suzuki, Ichiro Masai, Il Hwan Kim, Scott H. Soderling, Atsushi Miyawaki, and Tomomi Shimogori

Transparent Methods

All recombinant DNA and animal experiments in this study were performed in accordance with guidelines of Research Ethic Section of RIKEN.

Probe cDNA constructs

For construction of reconstitution probe, full-length Superfolder GFP (sfGFP) cDNA was synthesized from published sequences(Cabantous et al., 2005; Pedelacq et al., 2006), except 11th β-sheet is same as EGFP. sfGFP split sites of 1-7/8-11, 1-10/11 are 157/158, 214/215 amino acid positions respectively. Single 11th β-sheet fragment is optimized for reconstitution (Cabantous et al., 2005) which DNA sequence is 5'-CGCGATCACATGGTCCTGCATGAGTATGTGAATGCCGCCGGGATCACT-3'. For generating GPI-anchored type probe molecules, sfGFP fragments were inserted between mouse preproacrosin signal peptide and mouse Thy-1 GPI-anchored domain cDNA, which were kindly donated by Dr. G. Kondoh (Kyoto University, Japan)(Kondoh et al., 1999). Spacer domains (its cDNA sequence is 5'-GGTGGAGGCGGTTCAGGCGGAGGTGGCTCTGGCGGTGGCGGATCG-3') and acidic leucine zipper domain (LZA) or basic leucine zipper domain (LZB)(O'Shea et al., 1993) were inserted between sfGFP fragment and GPI-anchored domain. Pre- and post-mGRASP cDNAs were synthesized by GeneArt Strings DNA Fragments (Thermo Fisher Scientific) from published sequences(Kim et al., 2012), except NheI sites were introduced to replace GFP fragment domains. For generating a transmembrane type molecule, pDisplay was used (Thermo Fisher Scientific). To label cell nucleus, human histone H2B (donated by Dr. T. Kanda (Aichi Cancer Center Research Institute, Japan))(Kanda et al., 1998) was fused to mCherry (donated by Dr. R. Tsien (UC San Diego, USA)), or Azurite(Mena et al., 2006) (synthesized from published sequences). To identify transfected cells, probe molecules were jointed to H2B-mCherry or H2B-Azurite with self-cleavable T2A peptide which DNA sequence is 5'-GAGGGCAGAGGAAGTCTTCTAACATGCGGTGACGTCGAGGAGAATCCTGGCCCA-3'. To label synaptic sites of transfected neurons, rat PSD95 (donated by Dr. S. Okabe (Tokyo University, Japan)) was fused to mCherry, and probe molecules were jointed to PSD95-mCherry with self-cleavable P2A peptide which DNA sequence is 5'-GGAAGCGGAGCTACTAACTTCAGCCTGCTGAAGCAGGCTGGAGACGTGGAGGAGAACCCTGGACCT-3'.

For zebrafish retina experiment, using Gibson Assembly (NEB), tdTomato that has zebrafish gap43 membrane targeting signal at the 5' end, P2A and n-GRAPHIC were connected in frame (MemtdTomato-P2A-n-GRAPHIC). TagBFP2(Subach et al., 2011) and c-GRAPHIC are connected via P2A in frame (TagBFP2-P2A-c-GRAPHIC).

Color variants of GFP fragments were synthesized by GeneArt Strings DNA Fragments or site directed mutagenesis. BFP (similar to BFP2(Park and Rhee, 2012)) type NT-fragment was

generated by 8 amino acid substitutions (I39N, T65S, Y66H, S72A, K105T, T128V, V150I, D115V) into sfGFP 1-7. YFP type CT-fragment was generated by T203Y into sfGFP 8-11.

Lentivirus expression system

Lentivirus expression system is as described(Miyoshi et al., 1998; Miyoshi et al., 1997). cDNA encoding probe molecule or nucleus color label was cloned into a pCSII-CMV-MCS vector. To produce lentivirus solution, the plasmid was co-transfected with the packaging plasmid (pCAG-HIVgp) and the VSV-G- and Rev-expressing plasmid (pCMV-VSV-G-RSV-Rev) into HEK293T cells by X-tremeGENE HP DNA Transfection Reagent (Roche).

Cell cultures

LLCPK1 cells (donated by Dr. S. Yonemura (RIKEN CDB, Japan)) were cultured in DMEM (low glucose, Wako) containing 10% fetal bovine serum (Serum Source International). LLCPK1 clonal cell lines which stably express probe molecules were generated by lentivirus infection and cell sorting. HEK293T cells (RIKEN Cell Bank) were cultured in DMEM (high glucose, Wako) medium containing 10% fetal bovine serum. All cell lines were cultured at 37 ºC under 5% CO_2.

Flow Cytometry

For analytical flow cytometry, culture medium of LLCPK1 cells were replaced to 5 mM EDTA/ phosphate-buffered saline (PBS) and cells were dissociated with pipetting. Dissociated cells were filtrated with 40 μm cell strainer (Thermo Fisher Scientific). After centrifugation (200 X *g*, 10 min) cells were resuspended into PBS, and the cell suspensions were subjected to flow cytometry. Flow cytometry and cell sorting were carried out on a FACSAria II (BD Biosciences). Flow cytometry data were analyzed with FlowJo.

Immunostaining of LLCPK1 cells

NT-probe expressing LLCPK1 cells were fixed with 4% PFA in PBS. After the fixation solution was replaced with PBS, the specimens were permeabilized with PBS containing 0.1% Triton X-100 for 5 min and blocked with PBS containing 3% bovine serum albumin (Sigma) for 30 min. The specimens were incubated with rabbit anti-GFP antibody (1:200) (MBL) for 1 h, washed with PBS, and incubated with donkey anti-Rabbit IgG antibody Alexa Fluor® 488 conjugate (1:500) (Thermo Fisher Scientific) for 30 min. All antibodies were diluted with PBS containing 3% bovine serum albumin.

Imaging of LLCPK1 cells

For time lapse imaging, cells were grown on glass-bottomed dish in DMEMgfp (Evrogen) containing 10% fetal bovine serum and GlutaMAX I (Thermo Fisher Scientific). For snap shot, LLCPK1 cells were fixed with 4% PFA in PBS, and the fixation solution was replaced with PBS. Almost all LLCPK1 images were collected with inverted microscopes Olympus IX-83 and Hamamatsu ORCA Flash 4.0 cameras. For color variation analysis (GFP and YFP), the spectrum analysis was carried out by lambda scan mode (step size: 5 nm, band width: 10 nm) of FV1000

laser confocal microscope (Olympus). For investigation of subcellular distribution of probe molecules, immunostained cells were subjected to confocal imaging with FV1000.

Quantification of GFP reconstitution activities: average of GFP intensity at cell-cell contact sites or plasma membrane were normalized with averages of nuclear fluorescent intensities of co-expressed H2B-mCherry (RFP) and H2B-Azurite (BFP).

Quantification of dissociated membrane retraction: since the most active membrane retraction was observed about 10 min after ion chelation, its velocity was calculated with time lapse images between 10-12 min after ion chelation. Nuclear centroids (N1, N2) of two cells of interest were decided by ellipse approximation of binarized H2B-mCherry or H2B-Azurite images. Membrane distance between cell pairs was decided with line scan of brightness in DIC images along N1N2 line segment. Membrane retraction velocity after disruption of adherence junctions depends on intercellular distance, therefore velocities were normalized with N1N2 distances. Cell pairs with 40-100 μm inter-nuclear distances were chosen for analysis.

Images were processed in ImageJ 2.0.0.

Label of mouse thalamocortical connection with GRAPHIC

In utero electroporation (IUE) of ICR mice were carried out as described previously(Matsui et al., 2013; Shimogori and Ogawa, 2008). For visualization of adult mouse neuronal connection, genome integrate system with Tol2 transposase(Sato et al., 2007) was used. cDNA encoding probe molecule and color label was cloned into a pT2K-CAGGS vector, and the plasmid was co-electroporated with pCAGGS-T2TP. All IUEs were done in the right side of embryonic mouse brains.

For AAV production, the AAV Helper Free System (Agilent Technologies) was used. The cDNA encoding the probe molecule and nucleic label (c-GRAPHIC-T2A-H2B-mCherry) was cloned into the pAAV-MCS vector (Agilent Technologies). To produce the recombinant AAV, pAAV- c-GRAPHIC-T2A-H2B-mCherry was co-transfected with pAAV-DJ/8 (Cell Biolabs), which supplies AAV2 replication proteins and AAV-DJ/8 capsid proteins, and pHelper (Agilent Technologies) which supplies the necessary adenovirus gene products required for the AAV production into the 293FT cell line (Thermo Fisher Scientific) utilizing the 293fectin transfection reagent (Thermo Fisher Scientific). After 72 h, the supernatant was collected and centrifuged at 2,000 × *g* for 30 minutes and then filtered through a 0.45 μm filtration unit (Millipore). Purification of the AAV was carried out by ultracentrifugation (87,000 × *g*, 2 h) with 20% sucrose cushion. The AAV was injected into the right side thalamus of electroporated adult mouse brains by stereotaxic injection (A/P -1.65 mm, M/L +1.80 mm from bregma, D/V -3.5 mm from the pial surface). Injection volume of AAV solutions was 500 nl/site, and the rate was 200 nl/min. After the injection, the needle was kept at the position for an additional 2.5 min before removal. These injection experiments were carried out with KDS Legato 130 (KD Scientific) and stereotaxic frame (Muromachi Kikai).

All electroporated and AAV injected ICR mice were anesthetized with a lethal dose of pentobarbitone, and the animals were transcardially perfused with 4% PFA in PBS. Their brains were collected and post fixed overnight at 4°C in 4% PFA in PBS. Fixed brains were sectioned in the coronal plane with vibratome Leica VT1000S at 100-120 µm. The sections were mounted with 10% glycerol in PBS. Their confocal images were collected with FV1200.

Quantification of colocalization of GRAPHIC signal (GFP) and PSD95-mCherry (RFP): 12 confocal images of electroporated S1 layer IV were taken from 2 mouse brains. Identification of overlapping regions of GFP and RFP were automatically calculated using the AND function in ImageJ (Version 2.0.0.). The number of GFP puncta overlapped with or without mCherry puncta were manually counted.

GRAPHIC signal in zebrafish retina

All the fish we used in this study were in the *roy* mutant background that lacks silvery iridophores(White et al., 2008). After 10 hours post fertilization, we maintained fish in 1x E3 medium containing 0.003% of 1-phenyl-2-thiourea (Nacalai) to prevent melanin formation.

To express n-GRAPHIC in zebrafish cone cells, a 3.2 kb vsx1 promoter(Randlett et al., 2013) and MemtdTomato-P2A-n-GRAPHIC cDNA were assembled in a Tol2 plasmid(Kawakami, 2007). To express c-GRAPHIC in off type bipolar cells, a 3.2 kb promoter fragment of the *guanine nucleotide-binding protein G(t) subunit alpha-2* (*gnat2*) gene(Kennedy et al., 2007) and TagBFP2-P2A-c-GRAPHIC cDNA were subcloned into a Tol2 plasmid.

The n- and c-GRAPHIC plasmids diluted in 1x Danieu's buffer at the concentration of 25 ng/µl and 50 ng/µl Tol2 transposase mRNA were co-injected into one-cell stage embryos.

At 5 dpf, we fixed larvae in PBS containing 4% PFA and 5% sucrose. After fixation, retinas were dissected and then mounted in 0.7% molten low melting point agarose in PBS on a coverslip with optic nerve head side down. After solidifying the agarose, the coverslip was flipped and placed on a drop of VECTOR SHIELD (Vector) on a slide glass with a spacer to prevent squeezing. Confocal images were acquired with Olympus FV1000 (Olympus). Obtained z-stack confocal images were processed using ImageJ 2.0.0 and AMIRA (FEI).

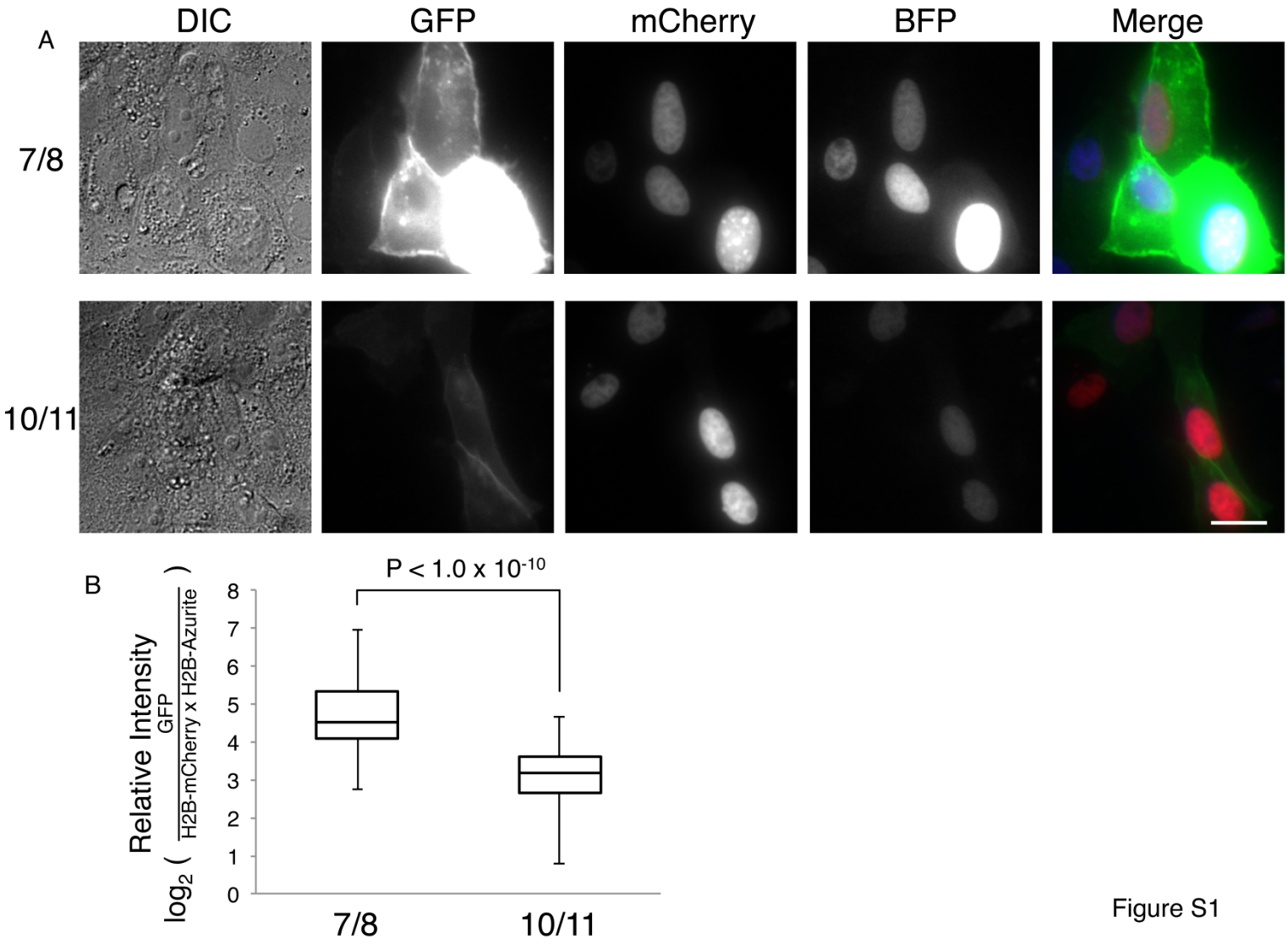
A
DIC
GFP
mCherry
BFP
Merge
7/8
10/11
B
P < 1.0 x 10-10
Relative Intensity
log2 (GFP / H2B-mCherry x H2B-Azurite)
8
7
6
5
4
3
2
1
0
7/8
10/11

Figure S1

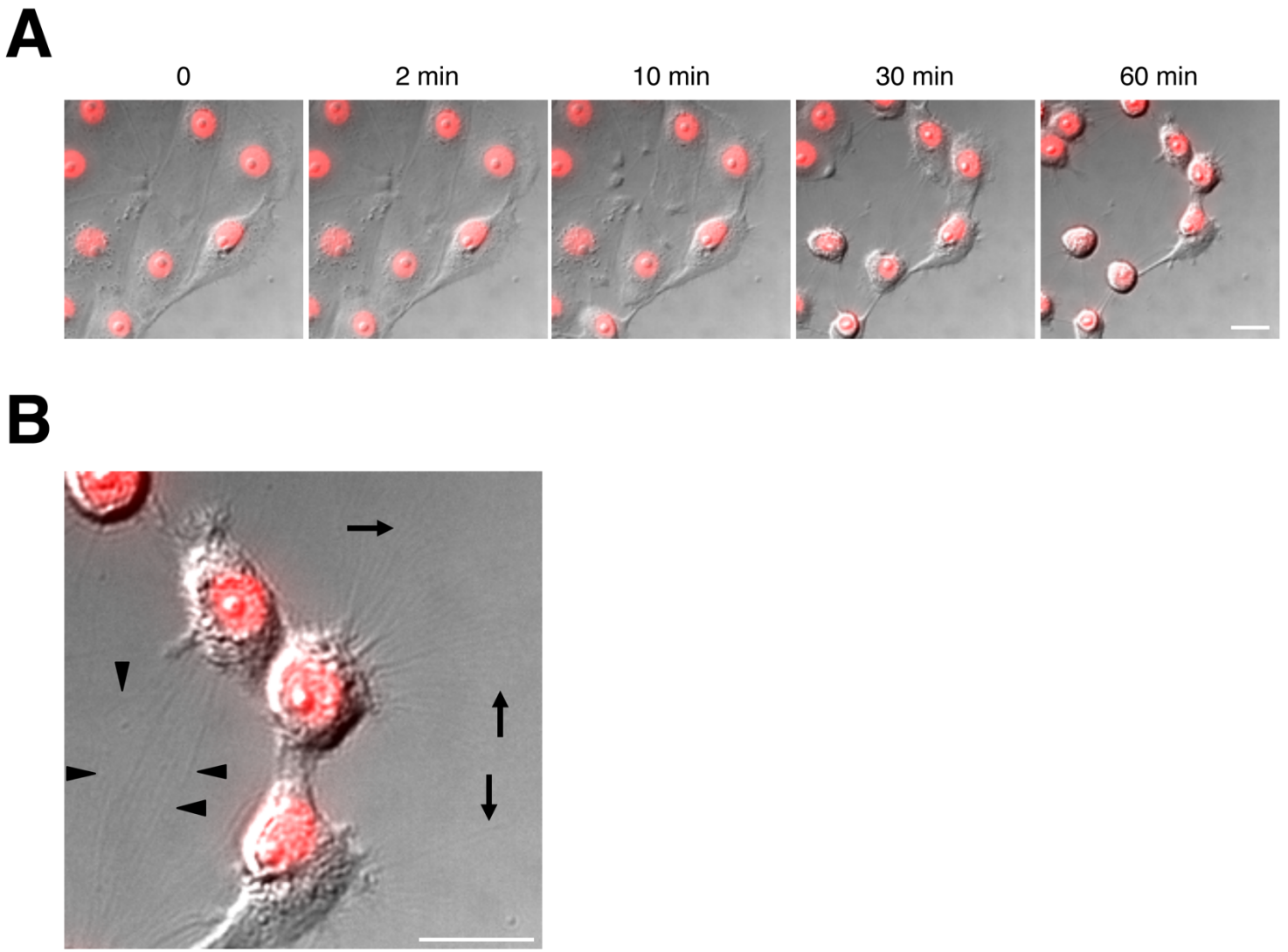
A
0
2 min
10 min
30 min
60 min
B

Figure S1. Comparison of reconstitution activity by different split site (related to Figure 1)

A. 7/8 split site of sfGFP showed more effective reconstitution activity than 10/11: To effectively label intercellular connection, we compared reconstitution activity of both 7/8 and 10/11 split sfGFP fragments. 7/8 split pair (GPI-sfGFP 1-7-2A-H2B-mCherry and GPI-sfGFP 8-11-2A-H2B-Azurite) or 10/11 split pair (GPI-sfGFP 1-10-2A-H2B-mCherry and GPI-sfGFP 11-2A-H2B-Azurite) were co-transfected into LLCPK1 cells. Co-expression of 7/8 split pair molecules showed strong reconstituted GFP signals, whereas co-expression of 10/11 split pair molecules showed relatively weak signals. **B.** Quantification and comparison of signal intensity of both spilt pairs indicates that 7/8 split pair (n =50) has more reconstitution activity than 10/11 split pair (n =60). GFP signals were normalized with co-expressed nuclei label intensities. $P = 1.23 \times 10^{-16}$; Student's unpaired t-test. Scale bar, 20 μm.

Figure S2 Ion chelation disrupt intercellular contact (related to Figure 3).

Time lapse images of control LLCPK1 cells in ion chelation experiment: To investigate the effect of GRAPHIC system on cell-cell adhesion, as a control experiment, we observed morphological changes of H2B-mCherry expressing (without GRAPHIC) LLCKP1 cells after disruption of adhesion junctions by ion chelation. (**a**) Time lapse images of control LLCPK1 cell morphology at each time points. EDTA was administrated at time 0 (final concentration; 5mM). Compared with GRAPHIC expressing cells (Fig. 2b), control cells did not show significant differences in cell morphology after ion chelation. (**b**) Higher magnification image of control cells at 60min after ion chelation. Fibers of plasma membrane were also observed at regions not previously associated with cell-cell contacts prior to ion chelation (arrows). Even at previous cell-cell contacting sites, some fibers did not connect to other cells (arrowheads). These time lapse images suggest that these fiber structures may not be largely caused by remains of cell-cell contacts but cell-substrate contacts (focal contacts). Scale bars, 20 μm.

Supplementary Movie 1. Dynamics of GRAPHIC signals during the establishment of intercellular contact of epithelial cells. (related to Figure 3A)

This movie shows the signal distribution of GRAPHIC and change in its intensity during establishment of the intercellular contact between n-GRAPHIC expressing LLCPK1 cells (red nuclei) and c-GRAPHIC expressing LLCPK1 cells (blue Nuclei). Length of video, 12 h.

Supplementary Movie 2. Dynamics of GRAPHIC signals in disruption of intercellular contact of epithelial cells. (related to Figure3B)

This movie shows dynamics in distribution and intensity of GRAPHIC signal when intercellular contact between n-GRAPHIC expressing LLCPK1 cells (red nuclei) and c-GRAPHIC expressing

LLCPK1 cells (blue Nuclei) is disrupted by ion chelation. Length of video, 1 h.